Bloch-Wave Engineering for High-Q, Small-V Microcavities

Ph. Lalanne and Jean Paul Hugonin

***Abstract*—The overall decay rate of the mode in an optical microcavity formed by a defect surrounded by two Bragg mirrors in a monomode waveguide is driven by two mechanisms, the desired coupling to a guided mode and the detrimental coupling to radiation modes. We propose two approaches fully compatible with planar fabrication, which allow to increase the cavity Q's by several orders of magnitude while keeping constant the mode volume V of the cavity. The first approach consists of engineering the mirror to taper the guided mode into the mirror Bloch mode, thus decreasing losses. The second approach is less intuitive and relies on a recycling mechanism of the radiation losses. The study is supported by computational results obtained for two-dimensional silicon-on-insulator geometries, but the results apply as well to other related geometries like three-dimensional photonic-wire cavities.**

***Index Terms*—Band gap, cavities, confinement, defect modes, emission, optical resonators, Q-factor.**

I. Introduction

ELECTROMAGNETIC resonant cavities, which trap light within a finite volume, are an essential component of many important optical devices and effects, from lasers to filters to single photon sources. Cavities are characterized by two main quantities: the modal volume V and the quality factor Q. In many applications, high Q's and small V's are highly desirable for the high finesse required for laser and filter applications and for the high Purcell factor [1] required for controlling the spontaneous emission of atoms placed in resonance with the microcavity mode [2]. Usually the refractive index contrast of dielectric layers is low (typically 1% for a distributed Bragg reflector (DBR) in guided wave configurations), and a large number of small reflections over a long propagation distance is needed to warrant high reflectivity [3]. Thus, high Q's are achieved at the expense of large V's. Alternatively, periodic microstructures deeply etched into a semiconductor waveguide offer high refractive-index contrasts and much shorter penetration lengths in the mirrors. Examples include photonic-wire microcavities [4], [5] and very compact Bragg reflectors [6]–[9]. However, for strong corrugations, the Bragg mirror cannot be considered as a perturbation of the uncorrugated waveguide, radiation losses in the claddings are inevitable, and the Q factor is lowered. Thus high Q's and small V's appear to be two conflictual objectives.

Let us quickly illustrate our purpose on the basic problem related to the reflection of a TE guided-wave impinging at normal incidence (z direction) from a monomode waveguide onto a one-dimensional (1-D) semi-infinite Bragg mirror, see the inset in Fig. 1. A silicon-on-insulator (SOI) waveguide, composed of a silicon (refractive index 3.48) 260-nm-thick core with claddings with respective refractive indices of 1 and 1.44, will be considered hereafter. Above $\lambda = 1.5$ μm, the waveguide supports a single guided mode. The first-order Bragg mirror has a period $\Lambda = 320$ nm and is composed of lamellar slits (width $w = 110$ nm) etched down to the SiO_2 substrate. The solid curve in Fig. 1 shows the calculated loss ($L = 1 - R$) spectrum, where R is the modal reflectivity, including the full band-gap region from 1.3 to 1.8 μm. Let us just imagine a cavity formed by a small defect length inserted between this two semi-infinite mirrors and resonating at a midgap frequency. For small defects lengths, the cavity number m (including the penetration depth in the mirrors) is ≈ 3 as will be shown hereafter by use of a Fabry–Perot model, and thus the intrinsic $Q = m\pi R^{1/2}/L$ is only ≈ 300.

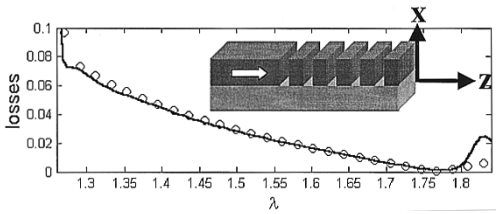

Fig. 1. Spectrum of the radiation losses resulting from the reflection of a guided wave on a semi-infinite Bragg mirror in the SOI waveguide (inset). The scattering problem is invariant along the y direction. Solid curve: computational results using electromagnetic theory. Circles: predictions of the approximate model in [12].

Theoretically, two approaches which lead to infinite Q's are known. The first one has motivated the concept of the three-dimensional (3-D) photonic crystal, the famous "cage for photons" [10]. The second refers to a subtle engineering of the core and cladding materials of the waveguide stack, so that no mode profile mismatch occurs when propagating through the different waveguide sections [11]. Both approaches require a sophisticated 3-D refractive-index engineering. The purpose of this paper is to propose two other routes, fully compatible with planar fabrication, which allow to increase the cavity Q's by several orders of magnitude while keeping constant cavity V's. The contribution is theoretical. In Section II, some Bloch-mode properties needed in the following are reviewed. In Section III, we use these properties to engineer nonperiodic mirrors which provide an "adiabatic" conversion and which exhibit small radiation losses. Microcavities are studied in Section IV. Section IV-A is devoted to microcavities formed by the association of two engineered mirrors. As expected,

Manuscript received April 16, 2003; revised August 5, 2003.

The authors are with the Laboratoire Charles Fabry de l'Institut Optique, Centre National de la Recherche Scientifique et Université Paris Sud, F-91 403 Orsay Cedex, France.

Digital Object Identifier 10.1109/JQE.2003.818283

the reduction of the radiation losses provided by the tapering enhances the Q/V factor by several orders of magnitude. Although this route has been previously validated numerically [12] and experimentally [9], the present study is more complete and provides a better physical understanding of the tapering effect. The second route, presented in Section IV-B, consists of engineering the full microcavity. In particular, we exploit the fact that the mirror losses can be recycled in very short microcavities by radiation modes. Section V provides a discussion of the different concepts and concludes the article.

Throughout the paper, the computational results are obtained with a frequency-domain Fourier modal method [13], [14]. In brief, the method relies on a supercell technique (artificial periodization in the transverse planes) and incorporates perfectly matched layers (PMLs) [15] to avoid electromagnetic contamination between adjacent cells. In every uniform longitudinal section of the cavity, the modes are computed exactly in a Fourier basis and a scattering matrix is used to recursively relate the mode amplitudes in every section. The Fourier expansion (also called plane-wave method in the field of photonic crystals) incorporates Fourier factorization rules [16] which drastically improve the convergence rate of the truncated Fourier expansions (for more details, see [17]–[20] where high performance with Fourier series are reported for grating-diffraction and photonic-band computations). For the TE-polarization case and for the two-dimensional (2-D) geometries we consider hereafter, the accuracy of the numerical results is rather high. For similar diffraction geometries, a six-digit accuracy for the computed modal reflectivity has been achieved with the present approach for a large number of retained Fourier harmonics (see [14, Table 1]). The numerical results reported here have been obtained for 81 retained Fourier harmonics, and the relative accuracy of all numerical data is expected to be better than a few percent. Bloch-wave computations are performed with the method of [13]. The refinement procedure of [21] is used to obtain enhanced stability and accuracy.

The following numerical results are all obtained for the same SOI waveguides. It is assumed that the grooves are etched down to the SiO_2 substrate, i.e., only the silicon layer is patterned. This assumption results in a simple binary etching process for which the SiO_2 substrate may be used as an etch stop.

II. Bloch Modes

We define the Bloch modes of a Bragg mirror (periodicity Λ along the z direction) as the solutions of Maxwell's equations for the periodic structure in the absence of illumination. Let us denote by $|\mathbf{B}\rangle = \begin{bmatrix} \mathbf{E}_t \\ \mathbf{H}_t \end{bmatrix}$ the Bloch-mode vector formed by the transverse components of the electric and magnetic fields. The Bloch modes are pseudo-periodic functions of z, which can be written

$$|\mathbf{B}\rangle = |\mathbf{B}'(x,y,z)\rangle \exp(jk_0 nz) \tag{1}$$

with $|\mathbf{B}'(x,y,z+\Lambda)\rangle = |\mathbf{B}'(x,y,z)\rangle$. In (1), k_0 is the modulus of the free-space wavevector and the quantity n represents the effective index of the Bloch mode. It is defined modulo $2\pi/(k_0\Lambda)$.

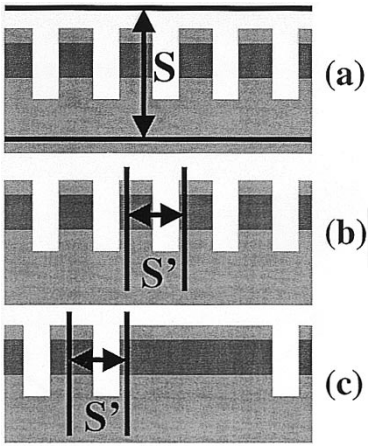

Fig. 2. Different approaches for Bloch-mode calculation of a periodic waveguide. (a) Grating approach: the Bloch modes are calculated as the complex pole of a "transverse" scattering matrix $\mathbf{S}$. (b) Waveguide approach: the Bloch modes are calculated as the eigenstates of a "longitudinal" scattering matrix $\mathbf{S}'$. (c) The same Bloch modes can be formally identified in a complex and nonperiodic waveguide structure.

Two different approaches are usually used to calculate the Bloch modes. As shown in Fig. 2(a), one may calculate the Bloch modes as the complex poles of the determinant of a "transverse" scattering matrix $\mathbf{S}$ that relates the electromagnetic field components in the substrate and in air. This approach has been used over many years in grating theory (see, for instance, [22] and references therein). Alternatively, one may also calculate the Bloch modes as the eigenstates of a "longitudinal" scattering matrix $\mathbf{S}'$ relating the electromagnetic fields between two planes separated by one period [see Fig. 2(b)]. These two approaches are mathematically equivalent. The interested reader may refer to [21] for a comparison of the performance of the two approaches and for a more quantitative discussion. Clearly, the first approach [Fig. 2(a)] emphasizes the periodic nature of the Bloch modes, whereas the second approach [Fig. 2(b)] refers to some locality: the Bloch modes are seen as the eigenstates of the scattering matrix associated with a specific segment. This segment may correspond to a single period of a periodic structure, as shown in Fig. 2(b), or may be embedded into a more complex and nonperiodic patterned waveguide, as shown in Fig. 2(c). As will be shown in Section III, the second approach allow us to emphasize the key role of Bloch modes in nonperiodic tapered mirrors.

Fig. 3(a) and (b) shows the classical dependence of the fundamental Bloch-mode effective index of a periodic waveguide as a function of the periodicity constant. The figure is obtained for the SOI waveguide previously discussed and for a fixed fill factor, $w/\Lambda = 110/320$. Unlike many recent works on band computations, where one finds the frequency for a fixed parallel wavevector $k_0 n$ in the Brillouin zone, the frequency was fixed for the computation ($\lambda = 1.56\,\mu$m) and the effective index was calculated as an eigenvalue. Over the full horizontal axis in Fig. 3(a) and (b), the fundamental Bloch mode is nonleaky. Consequently, effective indices with nonnull imaginary parts represent nonpropagating Bloch modes operating in the band-gap region. $\mathrm{Im}(n)$ is directly related to the inverse of the penetration length in the mirror [23]. The Bloch modes are composed of a

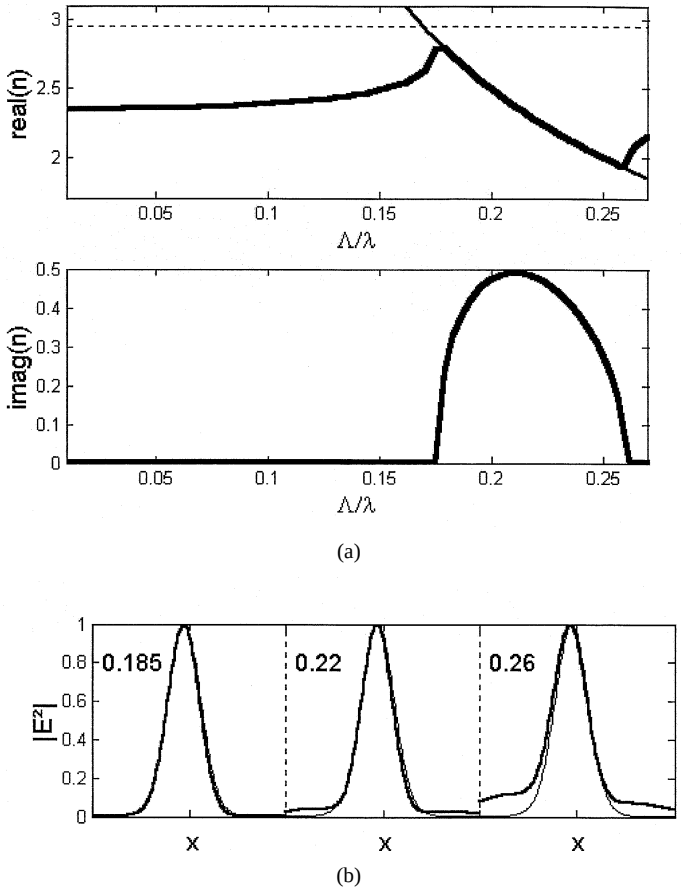

Fig. 3. Calculated Bloch modes and effective indices for the SOI Bragg mirror, as a function of the periodicity constant Λ. The frequency and the fill factor are fixed, $\lambda = 1.56\ \mu$m, and $w/\Lambda = 110/320$. (a) $\mathrm{Re}(n)$ as a function of Λ. The horizontal dashed line represents the effective index of the unpatterned SOI waveguide. The thin solid curve is $\Lambda/2\lambda$. (b) $\mathrm{Im}(n)$ as a function of Λ. (c) Transverse profile along the x direction (squared electric-field magnitude) of the half-Bloch waves for three periods $\Lambda/\lambda = 0.185$, 0.22, 0.26 covering the bandgap region. Thin curves represent the transverse profile of the guided mode of the unpatterned waveguide. They are all identical.

superposition of waves propagating in the positive and negative z directions, called half-Bloch waves in the following. Within the gap, these waves are back-coupled through a multiple p of the grating vector $2\pi/\Lambda\mathbf{z}$ and, thus, $\mathrm{Re}(n)$ approximately verifies the grating equation

$$\mathrm{Re}(k_0 n) - p\frac{2\pi}{\Lambda} = -\mathrm{Re}(k_0 n). \tag{2}$$

Note that (2) is strictly satisfied for periodic thin-film stacks [23]. The values of $\mathrm{Re}(n)$ provided by (2) for the first band gap $(p = 1)$ are represented in Fig. 3(a) by the thin solid curve. They are found to be in excellent agreement with the calculated data over the full band gap.

III. Engineered Mirrors

In this section, we show that, by engineering the mirror geometry, it is possible to drastically reduce the losses at the interface between a Bragg mirror and a z-invariant waveguide. This reduction is achieved by a gradual variation of the mirror geometry (see Fig. 4) aimed at tapering the incident guided mode into the fundamental Bloch mode of the mirror. Because our motivation is to design short mirrors which could be used for microcavities, the tapered mirrors have to be very short, typically one wavelength long.

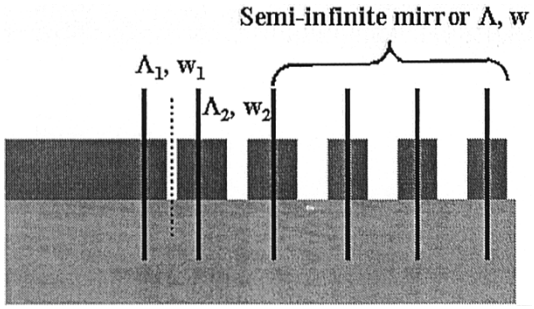

Fig. 4. Geometry of the tapered mirrors. Two segments, length Λ_i and slit width w_i, are inserted between the semi-infinite mirror and the z-invariant waveguide. Note that all the segments possess a symmetry relatively to a vertical plane located in the slit center (vertical dotted line).

In integrated optics, gradual variation of patterned waveguides has previously been investigated for mode transformation. Tapered "segmented waveguides" which relies on a very progressive transformation of the so-called "quasi-modes" have been proposed and implemented for independently controlling the vertical and lateral confinements [24]–[26] in optical waveguides. More recently, short tapers for coupling into photonic crystal waveguides have also been proposed [27]–[29] and implemented [30]. All these works rely on an engineering of propagating Bloch modes. Although its principle of operation shares common features with these previous works, our approach is radically different since we aim at engineering nonpropagative Bloch operating in the band gap. With the exception of the works in [9], [12], and [31], this problem is untreated in the literature to our knowledge.

A. The Impedance-Mismatch Problem

A physical interpretation for the loss origin involved at the interface between a classical waveguide and a semi-infinite Bragg mirror has been first proposed in [12]. The interpretation relies on a semi-analytical model which gives evidence that the losses originate from an impedance mismatch between the fundamental guided mode of the z-invariant waveguide and the (nonpropagating) fundamental Bloch mode of the Bragg mirror. More specifically, the losses are understood as resulting from a triple scattering process. The incident guided waveguide is first scattered into the fundamental half-Bloch wave propagating into the positive z direction (with some losses into radiation modes), then this wave is coupled back into the counterpropagating half-Bloch wave and finally is scattered back into the conventional waveguide. Provided that the fundamental Bloch mode is a genuine nonleaky guided mode, the back-coupling is performed with a unitary efficiency, and the radiation losses only result from a mode mismatch. These losses L vary linearly with the square of the overlap integral η between the fundamental guided and the half-Bloch wave associated with the fundamental Bloch mode of the Bragg mirror, $L = 1 - \eta^2$[12]. The model predictions has been validated for many waveguide geometries and

polarizations [12]. For the SOI waveguide previously studied, they are represented by circles in Fig. 1 and are found to be in excellent agreement with the rigorous numerical results (solid curve).

From Fig. 1, we note that the radiation losses increase with decreasing wavelength inside the band gap. This effect can be simply understood. As the period increases in the gap or equivalently as the wavelength decreases, the Bloch mode becomes less and less confined in the high index material. This effect results in a decrease of the effective index as the wavelength decreases, see Fig. 3(a), and also as shown in Fig. 3(c), in an increased difference between the half-Bloch wave and the guided mode. As a whole, as the wavelength decreases in the gap, the overlap integral between the incident guided mode and the half-Bloch wave decreases and the impedance-mismatch problem becomes more severe.

B. Nonperiodic Mirrors for Modal Conversion

The impedance mismatch problem shows the necessity of designing mirrors which incorporate modal conversion to reduce the radiation losses. Following [12], we study segmented tapers which are formed by a series of etches whose feature dimensions vary progressively. A mirror incorporating two segments between the z-invariant waveguide and the semi-infinite periodic Bragg mirror is shown in Fig. 4. As will be shown hereafter, the art of obtaining nearly lossless short mirrors lies in tapering the guided mode of the unpatterned waveguide into the fundamental Bloch mode of the Bragg mirror.

Although hand-driven designs relying on a pure engineering of the eigenstates of the different segments have proven successful [32], we rather resort here to optimization relying on electromagnetic theory. For the design, all the segments are assumed to possess a symmetry relatively to a vertical plane located in the slit center. For every case, the optimizations are performed for mirrors composed of a semi-infinite mirror ($\Lambda = 320$ nm and $w = 110$ nm) engineered with one, two, and three segments. Simulated annealing [33] was used to maximize the modal reflectivity at a midgap wavelength $\lambda = 1.56$ μm. The loss and reflectivity spectra are shown in Fig. 5(a) and (b), respectively. The segment geometries are given in the figure caption. The numerical results clearly evidence the beneficial effect of inserting segments: over the full bandgap region, the mirror losses decrease with increasing number of segments. This is especially stringent at the wavelength of design. Relatively to the classical mirror, a loss reduction by more than a factor of 200 is achieved for the three-segment engineered mirror.

C. One Bloch-Mode Model

It is of interest to understand the loss reduction provided by the nonperiodic mirrors in terms of a Bloch-mode engineering process. To that purpose, we develop an approximate model, called one-Bloch mode model hereafter, which evidences the main physical mechanism leading to the loss reduction. The model can be applied to fully aperiodic Bragg reflectors for which the Bloch modes are nonpropagating, or to segmented waveguides for which modal conversion is achieved through propagating Bloch modes.

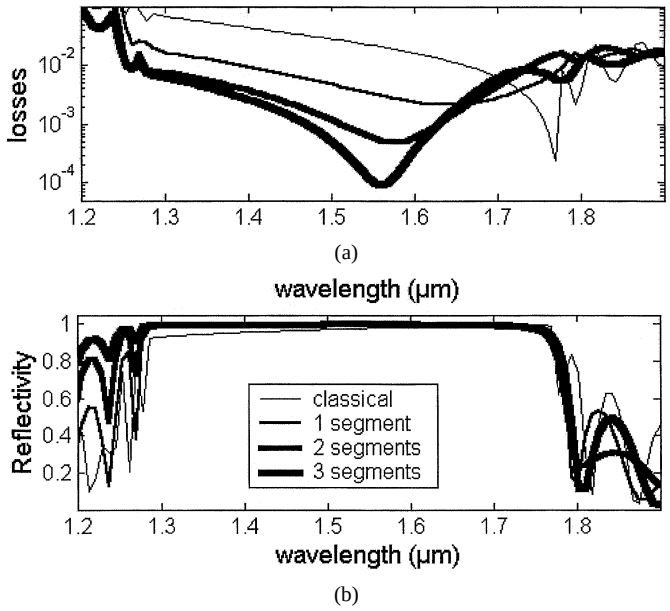

Fig. 5. Performance of the engineered mirrors. (a) Mirror losses. (b) Modal mirror reflectivities. As the number of tapered segments increases from 0 to 3, the corresponding curves become thicker. Classical mirror: $(w_i, \Lambda_i) = (110,320)$ nm, $\forall\ i$. One-segment engineered mirror: $(w_1, \Lambda_1) = (65,249)$ nm and $(w_i, \Lambda_i) = (110,320)$ nm, $\forall\ i \neq 1$. Two-segment tapered mirror:$(w_1, \Lambda_1) = (52,294)$ nm, $(w_2, \Lambda_2) = (95,249)$ nm and $(w_i, \Lambda_i) = (110,320)$ nm, $\forall\ i \neq 1,2$. Three-segment tapered mirror:$(w_1, \Lambda_1) = (49,247)$ nm, $(w_2, \Lambda_2) = (88,282)$ nm, $(w_3, \Lambda_3) = (102,264)$ nm and $(w_i, \Lambda_i) = (110,320)$ nm, $\forall\ i \neq 1,2,3$.

Let us consider the diffraction geometry shown in Fig. 4, and let us assume that the engineered mirror is illuminated by the fundamental guided mode of the z-invariant waveguide. Because Maxwell's equations are linear, the resolution of this diffraction problem amounts to estimate the transfer matrix $\mathbf{P}$ associated to the semi-infinite stack. With obvious notations, $\mathbf{P}$ can be written

$$\mathbf{P} = \mathbf{T}_1 \mathbf{T}_2 \mathbf{T}^{\infty} \tag{3}$$

where $\mathbf{T}_i$ is the transfer matrix associated with segment i, $\mathbf{T}$ is the transfer matrix associated with one period of the periodic mirror and $\mathbf{T}^{\infty} = \lim(\mathbf{T}^N)$ for $N \to \infty$. This limit exists provided that the frequency of the incident guided wave is in the band gap. Because every segment possesses an inversion symmetry, the $\mathbf{P}$ matrix can be rewritten as

$$\mathbf{P} = \boldsymbol{\Omega}_1 \begin{bmatrix} \boldsymbol{\Lambda}_1 & \mathbf{0} \\ \mathbf{0} & \boldsymbol{\Lambda}_1^{-1} \end{bmatrix} \boldsymbol{\Omega}_1^{-1} \boldsymbol{\Omega}_2 \begin{bmatrix} \boldsymbol{\Lambda}_2 & \mathbf{0} \\ \mathbf{0} & \boldsymbol{\Lambda}_2^{-1} \end{bmatrix} \boldsymbol{\Omega}_2^{-1} \cdot \left(\boldsymbol{\Omega} \begin{bmatrix} \boldsymbol{\Lambda} & \mathbf{0} \\ \mathbf{0} & \boldsymbol{\Lambda}^{-1} \end{bmatrix} \boldsymbol{\Omega}^{-1} \right)^{\infty}. \tag{4}$$

As shown in the Appendix, the matrices $\boldsymbol{\Omega}_1$, $\boldsymbol{\Omega}_2$, and $\boldsymbol{\Omega}$ are related to the eigenstates (or Bloch modes) of the different segments of the tapered mirror and the matrices Λ_i are diagonal matrices whose coefficients are directly related to the effective

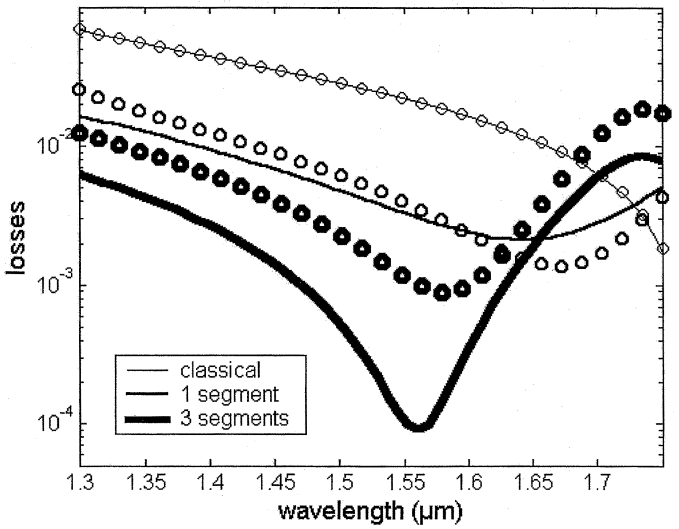

Fig. 6. Comparison between the one-Bloch-mode model and exact computational results for the engineered mirrors. The mirror characteristics are defined in the caption of Fig. 5.

indices of the Bloch modes of the segments. To evidence the key role played by the fundamental Bloch mode of every segment in the loss reduction, we consider the transfer matrix $\mathbf{P}'$

$$\mathbf{P}' = \boldsymbol{\Omega}_1 \begin{bmatrix} 0 & & & & \\ & \lambda_1 & & \mathbf{0} & \\ & & 0 & & \\ & & & 0 & \\ & \mathbf{0} & & \lambda_1^{-1} & \\ & & & & 0 \end{bmatrix} \boldsymbol{\Omega}_1^{-1} \cdot \boldsymbol{\Omega}_2 \begin{bmatrix} 0 & & & & \\ & \lambda_2 & & \mathbf{0} & \\ & & 0 & & \\ & & & 0 & \\ & \mathbf{0} & & \lambda_2^{-1} & \\ & & & & 0 \end{bmatrix} \boldsymbol{\Omega}_2^{-1} \cdot \left(\boldsymbol{\Omega} \begin{bmatrix} 0 & & & & \\ & \lambda & & \mathbf{0} & \\ & & 0 & & \\ & & & 0 & \\ & \mathbf{0} & & \lambda^{-1} & \\ & & & & 0 \end{bmatrix} \boldsymbol{\Omega}^{-1} \right)^{\infty} \quad (5)$$

where only the eigenvalues λ_i and $1/\lambda_i$ corresponding to the fundamental Bloch modes propagating in the positive and negative z directions of every segment are considered (all the other diagonal terms are set to zero). In this way, the energy transfer through every segment is solely ensured by the fundamental Bloch mode of the corresponding segment, while the energy exchange at the segment boundaries is carefully taken into account by retaining all the possible Bloch modes in the matrices $\boldsymbol{\Omega}$. Although transfer matrices are used here for the schematic description of the one-Bloch mode model, scattering matrices linking incident waves to diffracted ones are used for the numerical computation for the sake of stability.

In Fig. 6, we compare the losses predicted by the one-Bloch-mode model (calculated using matrix $\mathbf{P}'$) with those predicted with exact electromagnetic theory (calculated using matrix $\mathbf{P}$) for the engineered mirrors. An overall good agreement is achieved over the full gap. Although it is not able to accurately predict small losses ($L < 10^{-3}$), the approximate model reflects all of the basic trends of the loss spectra, and especially the strong loss reduction for $\lambda = 1.56$ μm. This agreement evidences the key role played by the fundamental Bloch modes of the successive segments in the tapering process. Fig. 7 illustrates the transversal mode profiles of the fundamental half-Bloch waves involved in the three-segment engineered mirror. Bold curves, from left to right, show the modulus of the electric field of the half-Bloch modes of the three segments, the last curve corresponding to the half-Bloch mode associated with the periodic semi-infinite mirror. Along the z direction of every segment, the Bloch-mode electromagnetic fields (and consequently the half-Bloch waves) vary. The transversal profiles shown in Fig. 7 are obtained in vertical cross-sectional planes represented by the solid lines in Fig. 4. The thin curves in Fig. 7 are all identical and correspond to the transverse profile of the guided mode of the z-invariant waveguide. All curves are shown for $\lambda = 1.56$ μm, i.e., for the design wavelength corresponding to minimum losses. A comparison of the set of curves evidences the progressive conversion between the incident guided mode and the Bloch mode of the semi-infinite mirror. This mode conversion reflects in the effective-index distribution for the Bloch modes of the four segments. From segment 1 to 4, the effective indices vary progressively: $n = 2.84$, $2.83 + 0.20i$, $2.68 + 0.36i$, and $2.44 + 0.49i$, the effective index of the fundamental mode of the SOI waveguide being 2.95. With the exception of the Bloch mode of the first segment, all the fundamental Bloch modes are non propagating. From segment 1 to segment 4, $\mathrm{Im}(n)$ and $\mathrm{Re}(n)$ are graded. The graded variation indicates that, as the incident guided wave enters the mirror, it is reflected and spreads into the air slits and into the low refractive-index claddings, as illustrated by the transverse profiles of Fig. 7.

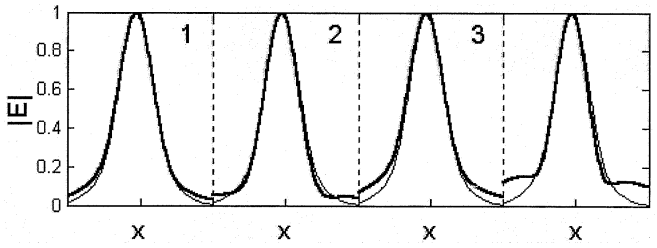

Fig. 7. Transversal profiles (modulus of the electric field) of the half-Bloch waves (bold curves) associated with the four segments of the three-segment tapered mirrors. From left to right, subplots labeled 1, 2 and 3 correspond to segments 1, 2, 3, respectively. The last curve corresponds to the half-Bloch wave associated to the periodic semi-infinite mirror. For the sake of comparison, the thin curves (they are all identical) represent the transverse profile (modulus of the electric field) of the fundamental guided wave. The wavelength is 1.56 μm.

Bloch-wave engineered surfaces for applications in free space or in integrated optics have already been manufactured for broad-band anti-reflection coating [34]–[36], high-performance blazing [37], confinement control [24]–[26], [28] and spectral apodization of Bragg gratings [38], [39]. All these approaches are concerned with propagating Bloch modes and a fill factor modulation is generally used for synthesizing the graded variation. In contrast, because we are concerned here

with nonpropagating Bloch modes operating in the gap, the segment period-to-wavelength ratio is the primary degree of freedom to be varied for the mode conversion. As shown by (2), it is directly related to the Bloch mode effective index in the gap and thus to the Bloch-mode profile.

IV. Microcavities

In this section, two different approaches for designing microcavities with high Q's and small V's are discussed. We first consider cavity incorporating engineered mirrors and, not surprisingly, the loss reduction is found to increase the cavity performance. The second approach is less intuitive and consists of engineering the full microcavity. In particular, we exploit the fact that, in cavities with small defect length, the mirror losses can be recycled by radiation modes [40].

The in-line microcavities studied hereafter are formed by inserting a short monomode waveguide section (length h), the default, between two identical Bragg mirrors. Before going into detail, let us briefly recall the main outcomes obtained from a Fabry–Perot model for symmetric cavities. The cavity transmission T_{cav} is given by the Airy formula [23], [3]

$$T_{\text{cav}} = \frac{T^2}{(1-R)^2 + 4R\sin^2\Phi} \tag{6}$$

where T and R are the modal transmission and reflection of the mirrors, and Φ is the total phase shift, $\Phi = 2\pi/\lambda\, n_{\text{eff}} h + \varphi$, φ being the mirror reflection phase and n_{eff} the effective index of the monomode waveguide mode. Under the assumption that T and R weakly depend on the wavelength, the Q factor $\lambda_0/\Delta\lambda$ of the cavity is $Q = m\pi\sqrt{R}/(1-R)$, with m being the cavity order [3], [9]

$$m = \left[\frac{2}{\lambda_0}\mathbf{n}_{\text{eff}}\mathbf{h} - \frac{\lambda_0}{\pi}\left(\frac{\partial\varphi}{\partial\lambda}\right)\lambda_0 - 2\mathbf{h}\left(\frac{\partial n_{\text{eff}}}{\partial\lambda}\right)\lambda_0\right]. \tag{7}$$

For a semi-infinite mirror, $T = 0$, therefore the coupling to radiation modes is the only decay mechanism which contributes to the overall decay rate of the cavity mode and the intrinsic cavity Q factor Q_I is $m\pi(R)^{1/2}/L$. Two other cavity parameters are important for applications: the maximum transmission $T_{\max} = [1 + L/T]^{-2}$ at resonance and the Purcell factor $F = (\lambda_0/n)^3\, Q/(4\pi V)$ [1] which describes the cavity capability to enhance the spontaneous emission rate of a perfect emitter phased with the cavity mode. Since V scales linearly with the cavity order, the factor Q/m (often called the finesse) is directly proportional to the Purcell factor. It will be used to describe the cavity capability to enhance the spontaneous emission rate in the following.

A. Microcavities With Optimized Mirrors

Since both the $T_{\max}$ and Q values depend on the coupling to radiation modes, one expects that cavities formed with the engineered mirrors of Section III offer improved performance in comparison with those obtained with periodic mirrors. Fig. 8 illustrates this improvement for the design wavelength $\lambda = 1.56\ \mu$m and for semi-infinite mirrors. As expected, the radiation loss reduction provided by the tapered mirrors result in an increase of the Q_I/m factor. The increase linearly scales with the loss reduction. Fig. 9 shows the transmission and reflection

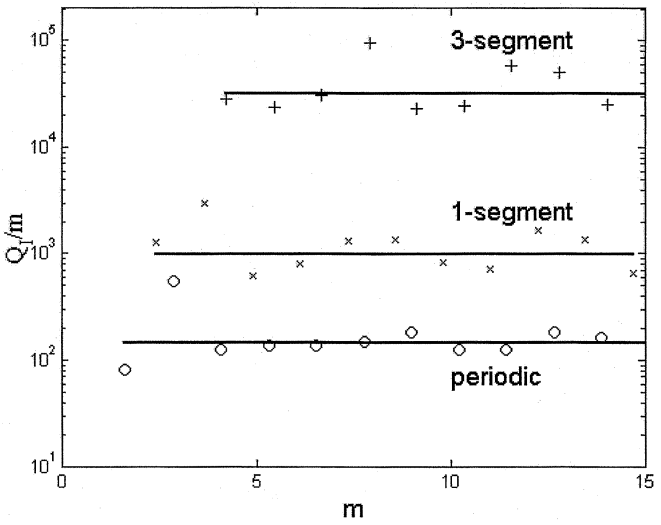

Fig. 8. Q_I/m ratio for microcavities formed by the association of two engineered mirrors. Circles, crosses, and plusses represent calculated Q_I/m ratio for cavities with periodic mirror, one-segment engineered mirror and three-segment engineered mirror, respectively. Horizontal bold lines represent the Q_I/m factor predicted with the Fabry-Perot model: $Q_I/m = \pi R^{1/2}/L$. Results hold for a resonance wavelength $\lambda = 1.56\ \mu$m.

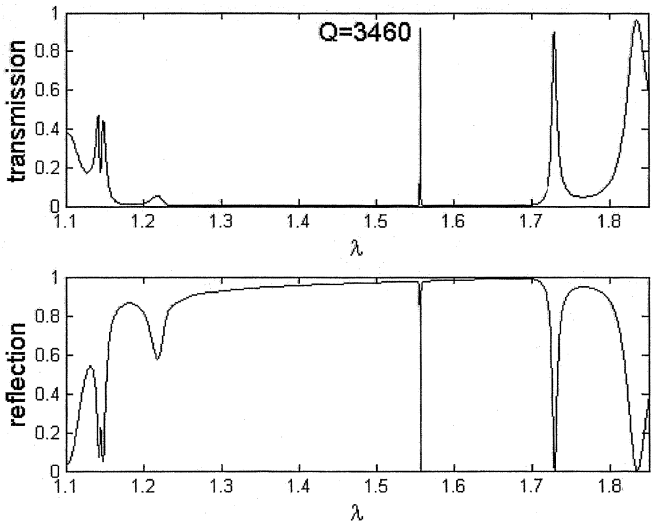

Fig. 9. Calculated transmission and reflection spectra for the symmetric cavity formed with the three-segment engineered mirror. The total number of grooves of the finite-length mirrors is seven.

spectra of a symmetric cavity ($h = 184$ nm) formed with the three-segment tapered mirror for four periodic segments. At resonance ($\lambda = 1.56\ \mu$m), $T_{\max} = 97\%$ and $Q = 3640$.

The horizontal bold lines in Fig. 8 represent the Q_I/m factors predicted with the Fabry–Perot model: $Q_I/m = \pi R^{1/2}/L$. Although the Fabry–Perot model well describes the basic trends of the Q_I/m factors, we observe a discrepancy between the calculated data and the Fabry–Perot model predictions. In fact, as shown in [40], the performance of microcavities with short defect length is not only driven by the modal mirror reflectivity and transmission, but also by a recycling of the radiation modes in the cavity defect, an effect on the spatial transient fields. When the recycling is phased with the cavity mode, the cavity Q is higher than the Fabry–Perot prediction. Conversely, dephasing results in lower Q's ("anti-recycling") [40].

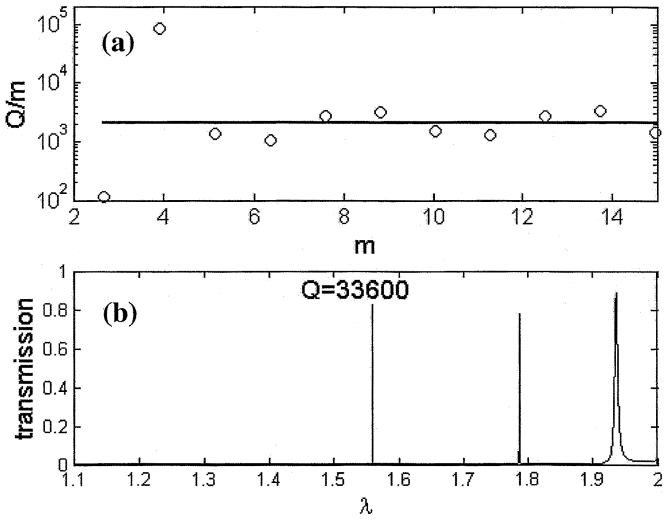

Fig. 10. Performance of the symmetric cavity with optimized recycling for $\lambda = 1.56\,\mu$m. The mirrors are formed by seven grooves with widths $w_i = 111$, 143, 175, 208, 241, 265 and 229 nm, separated by ridges of lengths 150, 158, 166, 170, 169, 173 nm. (a) Calculated Q/m factor as a function of m for $\lambda = 1.56\,\mu$m. The horizontal bold line represents the Q/m factor predicted with the Fabry–Perot model. (b) Transmission spectrum for $h = 140$ nm $(m \approx 4)$.

B. Microcavities With Optimized Recycling

Through simulated annealing [33], we have optimized cavity geometries formed by two symmetric mirrors with $N = 4$, 5, 6 and 7 grooves to enhance the recycling. The goal of the optimization procedure was to achieve simultaneously high Q/m and $T_{\max}$ values for a resonant wavelength $\lambda = 1.56\ \mu$m. For the optimization, all available degrees of freedom w_i, Λ_i ($i = 1$ to N) and h were varied. For every N value, cavity geometries providing enhanced recycling for small defect lengths were obtained. The trend is a $T_{\max}$ value nearly independent of N ($T_{\max} \approx 90\%$) and an increase of Q/m with increasing N values, basically due to the fact that larger N values allow for higher mirror reflectivities, and thus higher Q's. Fig. 10 shows the performance of the microcavities formed for $N = 7$ values. Fig. 10(a) shows the dependence with m of the Q/m factor for $\lambda = 1.56\ \mu$m and evidences the boost of the Q/m factor achieved by the recycling for $h = 140$ nm $(m \approx 4)$. The high Q/m value is nearly two-orders of magnitude larger than the Fabry–Perot model prediction, bold horizontal line in the figure. In addition, we note the strong "anti-recycling" achieved for small m. Similar strong recycling have also been predicted for 3-D air-bridge microcavities [40]. Fig. 10(b) shows the transmission spectrum of the cavity for $h = 140$ nm. It shows a single resonance ($T_{\max} = 89\%$ and $Q \approx 33\,600$) over a broad spectral interval from 1.1 to nearly 1.8 μm.

V. Discussion and Conclusion

We have explored two new routes, fully compatible with planar fabrication, which allow to increase the Q factors of optical microcavities by several orders of magnitude while keeping constant the mode volume of the cavity. The first route consists in engineering the Bloch modes of the mirrors in order to reduce the radiation losses occurring at the interface between the Bragg mirror and the classical waveguide. In this approach, we provided a thorough analysis of the loss-reduction mechanism and showed that the Bloch modes associated with the different segments of the engineered mirrors play a crucial role. The second route exploits a less intuitive mechanism, namely a recycling of the mirror losses through radiation modes excited at the interface between the unpatterned waveguide and the Bragg mirror. Calculations for optimized structures show that these two routes provide Purcell-factor enhancement by several orders of magnitude. Note that these two routes must not be opposed and can be combined in designs as evidenced by calculations obtained for 3-D air-bridge microcavities [40]. We performed many other calculations not reported in this paper for the sake of clarity and conciseness, and, in general, we observed that the cavity Q and the Purcell factor increase as the number of degrees of freedom retained for the optimization increases. This observation holds for cavities incorporating engineered mirrors, optimized recycling or a combination of the two processes. We have not performed lengthy optimizations for very large numbers of degrees of freedom and thus we do not know the ultimate theoretical performance for these cavities.

In practice, however, material absorption and inevitable residual scattering due to material inhomogeneities or surface roughness are likely to deteriorate the theoretical microcavity performance. Additionally, fabrication fluctuations are of importance. A first issue is the nonverticality of the groove walls provided by some residual over-etch, under-etch, or a combination of the two. We have not investigated this possibility, but previous numerical studies [41] performed for groove walls with a parabolic shape have revealed that etch errors are not a critical issue. Another important issue is the lithographical error leading to a discrepancy between the nominal slit widths and the fabricated ones. Therefore, we conducted some investigation of its effect. Although the lithographical error is likely to vary with the slit width, for the computations, we assumed that the deviation ΔL between nominal (w_i) and actual values $(w_i + \Delta w_i)$ is independent of the groove considered: $\Delta w_i = \Delta L$. In addition, we assumed that the fabrication process does not produce fluctuations of the spacing between two adjacent groove centers, an assumption largely valid for the lithographic process. Calculations were first performed for the cavity studied in Fig. 9 formed with two identical three-segment tapered mirrors ($Q = 3460$, $T_{\max} = 97\%$). We found that an increase of the slit width of $\Delta L = 10$, 20 nm corresponds to a decrease of $T_{\max}$, ($T_{max} = 83\%$, 64%) and an increase of the Q factor ($Q = 5200$, 7000). Conversely, we found that a decrease of the slit width of $\Delta L = -10, -20$ nm has nearly no impact on the peak transmission ($T_{\max} = 95\%$, 95%) and correspond to a decrease of the Q factor ($Q = 2100$, 1250). The trend is easily understood with a Fabry–Perot model if one considers that a positive (negative) value of ΔL basically corresponds to an increase (decrease) of the modal reflectivity of the mirrors. Trends for the cavity with optimized recycling ($Q = 33\,600$, $T_{\max} = 89\%$) of Fig. 10 are different: both positive or negative ΔL values correspond to a degradation of the $T_{\max}$ and Q factors. Typical degradations for the Q's by factors ≈ 2 and ≈ 6 are predicted for $\Delta L = \pm 10$ nm and ± 20 nm, respectively. For $\Delta L = 10$ nm and -10 nm,

the calculated $T_{\max}$ values are 20% and 60%. At first sight, the decrease of $T_{\max}$ might appear enormous, but one has to remember that this cavity offers a very high Q factor.[1] Thus, for these recycling-optimized microcavities, the best performance is achieved for the nominal parameters. This trend, which is completely different from the one observed for the tapered mirrors, is not surprising, especially if one considers that optimizing the recycling consists of optimizing the full cavity. This first attempt at tolerancing the device suggests that an optimal device given fabrication constraints may lead to significantly different results.

Subwavelength patterns manufactured with aspect ratios of about 4, with dimensions in the 100-nm range and with a 20-nm accuracy, are at the frontier of today nanofabrication facilities. However, microcavities with tapered mirrors consisting of slits with widths from 50 to 100 nm have been previously manufactured [9] into an SOI waveguide for operation at telecommunication wavelengths and have shown better performance than microcavities formed with periodic mirrors. In this previous work, the defect length was about ten wavelengths in the material and the recycling was negligible. In addition, fill factor modulation, instead of periodicity modulation as we recommended in this work, was used for the design of the engineered mirrors, resulting in three time longer tapers than those obtained in this work. Thus, it appears reasonable to anticipate that much better performance could be achieved experimentally in the future compared to the current published results, and we hope that the physically driven designs performed in this work will be helpful. In addition, we expect that other microcavity geometries, like micropillars [2] or 2-D photonic-crystal cavities etched in semiconductor membrane [42] could benefit from this kind of approach.

Appendix
Bloch Modes of Symmetric Segments

The purpose of this Appendix is to demonstrate the specific form used in (4) for the transfer matrix of segments with an inversion symmetry. Let us first briefly consider the transfer matrix of a segment of length L in a z-invariant waveguide. The result is classical. If we denote by $\mathbf{E}_M$ and $\mathbf{H}_M$ the matrices formed by the electric- and magnetic-fields transverse components of the radiation and guided modes, the transfer matrix $\mathbf{T}$ can be written [3]

$$\mathbf{T}=\begin{bmatrix}\mathbf{E}_M & \mathbf{E}_M\\ \mathbf{H}_M & -\mathbf{H}_M\end{bmatrix}\begin{bmatrix}\mathbf{\Lambda} & \mathbf{0}\\ \mathbf{0} & \mathbf{\Lambda}^{-1}\end{bmatrix}\begin{bmatrix}\mathbf{E}_M & \mathbf{E}_M\\ \mathbf{H}_M & -\mathbf{H}_M\end{bmatrix}^{-1} \tag{A1}$$

where Λ is a diagonal matrix whose diagonal coefficients are simply $\exp(jk_0\, n_{\text{eff}}^m\, L)$, $n_{\text{eff}}^{(m)}$ being the effective index of the mth guided or radiation mode.

Let us now consider a patterned segment in the same waveguide, like segment 1 in Fig. 4. We assume that this segment possesses an inversion symmetry represented by the vertical dotted line. Let us denote by the vector $|\mathbf{B}\rangle=\begin{bmatrix}\mathbf{E}_B\\ \mathbf{H}_B\end{bmatrix}$ an eigenstate of the transfer matrix $\mathbf{T}'$ of the segment with eigenvalue $\lambda(\mathbf{T}'|\mathbf{B}\rangle=\lambda|\mathbf{B}\rangle)$. Provided that the materials in the segment are reciprocal, time reversibility is guaranteed, and because of the inversion symmetry, we have

$$\mathbf{T}'\,(\lambda|\mathbf{B}'\rangle)=|\mathbf{B}'\rangle \tag{A2}$$

for $|\mathbf{B}'\rangle$ defined by $|\mathbf{B}'\rangle=\begin{bmatrix}\mathbf{E}_B\\ -\mathbf{H}_B\end{bmatrix}$. Equation (A2) implies that $|\mathbf{B}'\rangle$ is an eigenstate of matrix $\mathbf{T}'$ and that the corresponding eigenvalue is $1/\lambda$. Thus, provided that the materials are reciprocal, if $|\mathbf{B}\rangle=\begin{bmatrix}\mathbf{E}_B\\ \mathbf{H}_B\end{bmatrix}$ is an eigenstate of the transfer matrix of a segment possessing an inversion symmetry, $|\mathbf{B}'\rangle=\begin{bmatrix}\mathbf{E}_B\\ -\mathbf{H}_B\end{bmatrix}$ is also an eigenstate of the same matrix. Consequently, the transfer matrix of any symmetric segment (patterned or not) can be written

$$\mathbf{T}=\begin{bmatrix}\mathbf{E}_B & \mathbf{E}_B\\ \mathbf{H}_B & -\mathbf{H}_B\end{bmatrix}\begin{bmatrix}\mathbf{\Lambda} & \mathbf{0}\\ \mathbf{0} & \mathbf{\Lambda}^{-1}\end{bmatrix}\begin{bmatrix}\mathbf{E}_B & \mathbf{E}_B\\ \mathbf{H}_B & -\mathbf{H}_B\end{bmatrix}^{-1} \tag{A3}$$

where $\mathbf{E}_B$ and $\mathbf{H}_B$ denote the matrices formed by the electric- and magnetic-fields transverse components of the eigenstates of the segment. According to Section II, $|\mathbf{B}\rangle$ or $|\mathbf{B}'\rangle$ also represent the Bloch modes associated with the periodic structure formed by a series of identical segments. In (A3), Λ is a diagonal matrix whose diagonal coefficients are simply $(\exp(jk_0\, n^{(m)}\,\Lambda), n^{(m)}$ being the effective index of the mth Bloch mode.

Equation (A1) relative to a z-invariant segment and (A3) relative to a segment with an inversion symmetry are formally identical. Thus, from (A3), the electromagnetic properties (far field reflectance and transmittance) of a fully nonperiodic patterned waveguide composed of a sequence of segments possessing all an inversion symmetry (an example is given in Fig. 4) can be understood as those of an artificial waveguide composed of z-invariant segments, whose radiation and guided modes are Bloch modes. The exchange of energy between the different Bloch modes along the wave propagation direction being simply related to the impedance matching between the Bloch modes at the segment terminations like it is the case classically with waveguides composed of z-invariant segments.

[1]Other calculations performed for 3-D in-line microcavities with an optimized recycling, see [40], and with Q's factor of several thousands instead of several tens of thousands like in the present example, have shown that deviations of $\Delta L=\pm 20$ nm for the hole diameters lead to a small degradation of 7% for the peak transmission.

References

[1] E. M. Purcell, "Spontaneous emission probabilities at radio frequencies," *Phys. Rev.*, vol. 69, p. 681, 1946.

[2] H. Yokoyama and K. Ujihara, *Spontaneous Emission and Laser Oscillation in Microcavities*. Boca Raton, FL: CRC Press, 1995.

[3] L. A. Coldren and S. W. Corzine, *Diode Lasers and Photonic Integrated Circuits*. New York: Wiley, 1995.

[4] J. P. Zhang, D. Y. Chu, S. L. Wu, W. G. Bi, R. C. Tiberio, R. M. Joseph, A. Taflove, C. W. Tu, and S. T. Ho, "Nanofabrication od 1-D photonic bandgap structures along a photonic wire," *IEEE Photon. Technol. Lett.*, vol. 8, pp. 491–493, 1996.

[5] J. S. Foresi, P. R. Villeneuve, J. Ferrera, E. R. Thoen, G. Steinmeyer, S. Fan, J. D. Joannopoulos, L. C. Kimerling, H. I. Smith, and E. P. Ippen, "Photonic-bandgap microcavities in optical waveguides," *Nature*, vol. 390, pp. 143–145, 1997.

[6] T. F. Krauss and R. M. De La Rue, "Optical characterization of waveguide based photonic microstructures," *Appl. Phys. Lett.*, vol. 68, pp. 1613–65, 1996.

[7] T. Baba, M. Hamasaki, N. Watanabe, P. Kaewplung, A. Matsutani, T. Mukaihara, F. Koyama, and K. Iga, "A novel short-cavity laser with deep-grating distributed bragg reflectors," *Jpn. J. Appl. Phys.*, vol. 35, pp. 1390–94, 1996.
[8] T. F. Krauss, O. Painter, A. Scherer, J. S. Roberts, and R. M. De La Rue, "Photonic microstructures as laser mirrors," *Opt. Eng.*, vol. 37, pp. 1143–48, 1998.
[9] D. Peyrade, E. Silberstein, P. Lalanne, A. Talneau, and Y. Chen, "Short bragg mirrors with adiabatic modal conversion," *Appl. Phys. Lett.*, vol. 81, pp. 829–831, 2002.
[10] E. Yablonovitch, "Inhibited spontaneous emission in solid-state physics and electronics," *Phys. Rev. Lett.*, vol. 58, pp. 2059–2062, 1987.
[11] J. Ctyroky, "Photonic bandgap structures in planar waveguides," *J. Opt. Soc. Amer. A*, vol. 18, pp. 435–441, 2001.
[12] M. Palamaru and P. Lalanne, "Photonic crystal waveguides: Out-of-plane losses and adiabatic modal conversion," *Appl. Phys. Lett.*, vol. 78, pp. 1466–69, 2001.
[13] P. Lalanne and E. Silberstein, "Fourier-modal method applied to waveguide computational problems," *Opt. Lett.*, vol. 25, pp. 1092–94, 2000.
[14] E. Silberstein, P. Lalanne, J. P. Hugonin, and Q. Cao, "On the use of grating theory in integrated optics," *J. Opt. Soc. Amer. A.*, vol. 18, pp. 2865–75, 2001.
[15] J. P. Bérenger, "A perfectly matched layer for the absorption of electromagnetic waves," *J. Computation. Phys.*, vol. 114, pp. 185–200, 1994.
[16] L. Li, "Use or fourier series in the analysis of discontinuous periodic structures," *J. Opt. Soc. Amer. A*, vol. 13, pp. 1870–76, 1996.
[17] P. Lalanne and G. M. Morris, "Highly improved convergence of the coupled-wave method for TM polarization," *J. Opt. Soc. Amer. A*, vol. 13, pp. 779–784, 1996.
[18] L. Li, "New formulation of the fourier modal method for crossed surface-relief gratings," *J. Opt. Soc. Amer. A*, vol. 14, pp. 2758–67, 1997.
[19] E. Popov and M. Nevière, "Grating theory: New equations in fourier space leading to fast converging results for TM polarization," *J. Opt. Soc. Amer. A*, vol. 17, pp. 1773–1784, 2000.
[20] P. Lalanne, "Effective properties and band structures of lamellar subwavelength crystals: Plane-wave method revisited," *Phys. Rev B*, vol. 58, pp. 9801–07, 1998.
[21] Q. Cao, P. Lalanne, and J. P. Hugonin, "Stable and efficient bloch-mode computational method for one-dimensional grating waveguide," *J. Opt. Soc. Amer. A*, vol. 19, pp. 335–338, 2002.
[22] E. Popov, "Light diffraction by relief gratings: A macroscopic and microscopic view," *Prog. Opt.*, vol. 31, pp. 139–187, 1993.
[23] P. Yeh, *Optical Waves in Layered Media*. New York: Wiley, 1988.
[24] Z. Weissman and A. Hardy, "2-D mode tapering via tapered channel waveguide segmentation," *Electron. Lett.*, vol. 28, pp. 1514–1516, 1992.
[25] D. Ortega, J. M. Aldariz, J. M. Arnold, and J. S. Aichison, "Analysis of quasimodes in periodic segmented waveguides," *J. Lightwave Technol.*, vol. 17, pp. 369–375, 1999.
[26] S. G. Johnson, P. Bienstman, M. A. Skorobogatiy, M. Ibanescu, E. Lidorikis, and J. D. Joannopoulos, "Adiabatic theorem and continuous coupled-mode theory for efficient taper transitions in photonic crystals," *Phys. Rev. E*, vol. 66, p. 066 608, 2002.
[27] T. D. Happ, M. Kamp, and A. Forchel, "Photonic crystals tapers for ultracompact mode conversion," *Opt. Lett.*, vol. 26, pp. 1102–04, 2001.
[28] P. Lalanne and A. Talneau, "Modal conversion with artificial materials for photonic-crystal waveguides," *Opt. Express*, vol. 10, pp. 354–359, 2002.
[29] P. Sanchis, J. Marti, J. Blasco, A. Martinez, and A. Garcia, "Mode matching technique for highly efficient coupling between dielectric waveguides and planar photonic crystals circuits," *Opt. Express*, vol. 10, pp. 1391–97, 2002.
[30] A. Talneau, P. Lalanne, M. Agio, and C. M. Soukoulis, "Low-reflection photonic crystal taper for efficient coupling between guide sections of arbitrary widths," *Opt. Lett.*, vol. 27, pp. 1522–24, 2002.
[31] A. S. Jugessur, P. Pottier, and R. M. De La Rue, "One-Dimensional periodic photonic crystal microcavity filters with transition mode-matching features, embedded in ridge waveguides," *Electron. Lett.*, vol. 39, pp. 367–369, 2003.
[32] E. Silberstein, "Généralization de la méthode modale de Fourier aux problèmes de diffraction en optique intégrée. Application aux convertisseurs modaux par ingénierie des modes de Bloch," Ph.D. dissertation, University Paris VI, Paris, France, 2002.
[33] E. Aarts and J. Korst, *Simulated Annealing and Boltzmann Machine*. New York: Wiley, 1989.
[34] P. B. Clapham and M. C. Hutley, "Reduction of lens reflexion by the moth eye principle," *Nature*, vol. 244, pp. 281–282, 1973.
[35] P. Lalanne and G. M. Morris, "Antireflection behavior of silicon subwavelength periodic structures for visible light," *Nanotechnology*, vol. 8, pp. 53–56, 1997.
[36] Y. Kanamori, M. Sasaki, and K. Hane, "Broadband antireflection gratings fabricated upon silicon substrate," *Opt. Lett.*, vol. 24, pp. 1422–24, 1999.
[37] P. Lalanne, S. Astilean, P. Chavel, E. Cambril, and H. Launois, "Blazed-binary subwavelength gratings with efficiencies larger than those of conventional èchelette gratings," *Opt. Lett.*, vol. 23, pp. 1081–1083.
[38] H. Sakata, "Sidelobe suppression in grating-assisted wavelength-selective couplers," *Opt. Lett.*, vol. 17, pp. 463–465, 1992.
[39] D. Wiesmann, C. David, R. Germann, D. Erni, and G. L. Bona, "Apodized surface-corrugated gratings with varying duty cycles," *IEEE Photon. Technol. Lett.*, vol. 12, pp. 639–641, 2000.
[40] P. Lalanne and J. P. Hugonin, "Radiation recycling in optical microcavities," submitted for publication.
[41] R. Jambunathan, "Design studies for distributed bragg reflectors for short-cavity edge-emitting lasers," *IEEE J. Quantum Electron.*, vol. 33, pp. 1180–89, 1997.
[42] J. Vuckovic, M. Loncar, H. Mabuchi, and A. Scherer, "Design of photonic crystal microcavities for cavity QED," *Phys. Rev. E*, vol. 65, p. 016608, 2002.

Ph. Lalanne was born in Dax, France. He is an Ancien Elève of the Ecole Normale Supérieure de Saint Cloud. He received the Agrégation de Sciences Physiques and the M.S. degrees in solid-state physics in 1986, the Ph.D. degree in physics in 1989, and the Habilitation à diriger les Recherches degree in 1996, all from the University of Orsay, Orsay, France.

Since 1989, he has been Scientist Researcher at Centre National de la Recherche Scientifique, Institut d'Optique, Orsay, France. His former research concerned numerous topics in information processing related to devices, systems, algorithms and architectures for parallel optical processing and interconnects. In 1994, during his sabbatical year at the Institute of Optics, Rochester, NY, he was engaged in diffractive optics. He has co-authored 50 publications in optical information processing, image processing, electromagnetic theory, diffractive optics, and integrated optics. His principal areas of research in optics concern diffraction, grating and waveguide theories, artificial materials, subwavelength structures, and electromagnetic wave propagation in metals and in photonic bandgap materials.

Dr. Lalanne received the Bronze Medal of Centre National de la Recherche Scientifique in 1993 and was awarded the Fabry de Gramont Prize from the Société Française d'Optique for his works in diffractive optics. He is a member of the European Optical Society, the Société Française d'Optique, the Optical Society of America, and the International Society for Optical Engineering.

Jean Paul Hugonin received the Agrégation de Mathématique in 1974 and the M.S. degree in Optics in 1975, the Doct. d'Etat ès Sciences degree in Physics in 1983 from the University of Orsay.

He is Ancien Elève of the Ecole Normale Supérieure de Saint Cloud. He is now Maître de Conférence at the University of Paris VI, Paris, France. His current research interests concern computational physics for various applications in image processing and in nanophotonics.